Theoretical Analysis of AlAs$_{0.56}$Sb$_{0.44}$ Single Photon Avalanche Diodes with High Breakdown Probability

Jamal Ahmed, Shiyu Xie, Baolai Liang, Xin Yi, Xiao Jin, Manoj Kesaria, John. P. R. David, *Fellow, IEEE,* and Diana L. Huffaker, *Fellow, IEEE*

Abstract—**Single photon avalanche diodes (SPADs) are key enabling technologies for a wide range of applications in the near-infrared wavelength range. Recently, AlAs$_{0.56}$Sb$_{0.44}$ (hereafter AlAsSb) lattice-matched to InP has been demonstrated for extremely low excess noise avalanche photodiodes (APDs) due to its large disparity between electron and hole ionization coefficients (α and β respectively). The α/β ratio also plays a role in Geiger mode operation as it affects the avalanche breakdown probability and hence detection efficiency. In this work, we theoretically investigate the performance of AlAsSb based SPADs. The probability of breakdown for electron-initiated Geiger mode operation increases more sharply with multiplication region width due to progressively more dissimilar ionization coefficients. In comparison with other common avalanche materials, such as InAlAs, InP and Si, our result also suggests that SPADs based on AlAsSb have a sharper breakdown probability than the other three materials under similar low overbias ratio. The calculated breakdown probability of 0.81 in AlAsSb is 0.18 and 0.28 higher than that of InAlAs/Si and InP respectively at 5% overbias ratio and with avalanche region width of 1500 nm.**

Index Terms— **Avalanche Breakdown Probability, Single Photon Avalanche Diode.**

I. INTRODUCTION

Single Photon avalanche diodes (SPADs) operating at near-infrared (NIR) wavelengths are of significant interest in several applications including quantum cryptography [1], CMOS circuit characterization [2] and eye-safe Light detection and ranging (Lidar) [3]. SPADs operate in the so-called Geiger mode biased above breakdown voltage V_{BD} with an overbias ratio $(V-V_{BD})/V_{BD}$. This is a metastable state as a single carrier pair generation can cause the device to

breakdown leading to a large current swing that can be easily detected by electronic circuitry.

SPADs are characterized by their single photon detection efficiency (SPDE) and dark count rate (DCR). The SPDE is the product of photon absorption efficiency and the probability of the generated electron-hole pair triggering an avalanche breakdown, termed the breakdown probability. The DCR mainly originates from tunneling dark currents through the avalanche region or traps triggering the avalanche breakdown. A large overbias ratio increases the SPDE but often at the expense of an increased DCR. It is well known that in linear mode Avalanche Photodiodes (APDs), a material with a large electron (α) and hole (β) ionization coefficients ratio gives rise to a lower excess noise performance [4]. A larger α/β ratio is also desirable in SPADs for Geiger mode operation as it gives rise to a much steeper breakdown probability as a function of overbias ratio (for the electron-initiated process) [5]. However, the DCR also increases with the overbias due to the increased tunneling current generation. For instance, Itzer *et al.* [6] reported that their InP SPAD has almost 10 times increase in DCR (from 8 kHz to 75 kHz) when the overbias ratio increases from 7.5% to 15% to achieve desired SPDE (from 18% to 37%). This significant increase in DCR is attributed to the field-assisted tunneling current [6]. Thus, a large α/β ratio can improve SPAD performance considerably by operating at a relatively low overbias, thereby reducing DCR while still maintaining high SPDE.

Currently, NIR SPADs are based on a separate absorption and multiplication (SAM) heterostructure [7]. Typically, these devices utilize InP or In$_{0.52}$Al$_{0.48}$As (hereafter InAlAs) as avalanche multiplication region and In$_{0.53}$Ga$_{0.47}$As (hereafter InGaAs) as the absorption region. Alternatively, silicon (Si) based SPADs with germanium (Ge) absorber have also been demonstrated for NIR wavelength range [8]. Both InP and InAlAs have broadly similar α and β and are thus not optimal for achieving high detection efficiency, whereas Si which exhibits a larger α/β ratio has a large lattice-mismatch with Ge making device fabrication challenging. Recently, a novel alternative avalanche material AlAs$_{0.56}$Sb$_{0.44}$ (hereafter AlAsSb) has been demonstrated to have a α/β ratio much larger than any other III-V semiconductor and even Si [9]. AlAsSb can be grown on InP substrate with a relatively large indirect bandgap of 1.55 eV and is thus compatible with
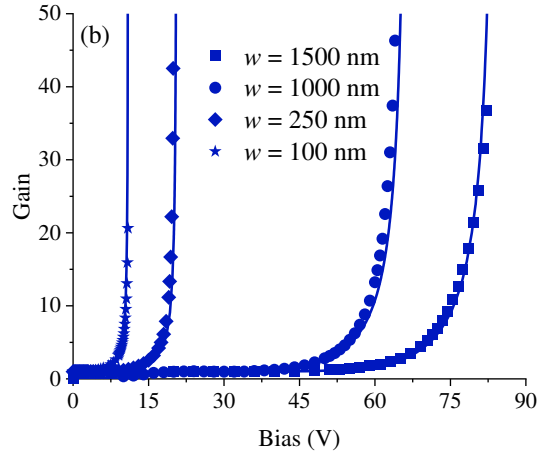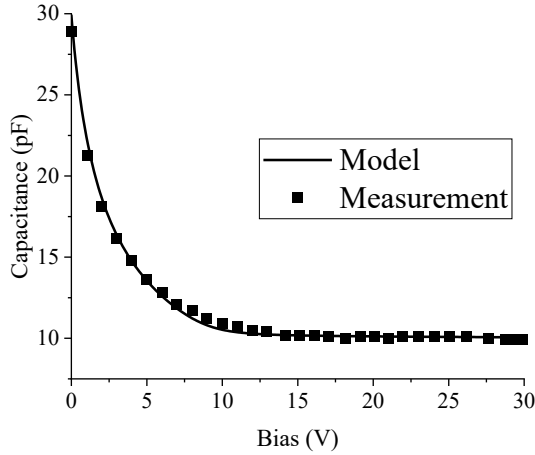
Fig. 1. (a) Measured (symbol) and modelled (line) C-V of AlAsSb p-i-n diode with w = 1000 nm. (b) Measured (symbols) and modelled (lines) multiplication gain for AlAsSb p-i-n diode with nominal w= 1500 nm (■), 1000 nm (●), 250 nm (◆) and 100 nm (★) at wavelengths of 420 nm.

existing InGaAs technology for 1310/1550 nm detection. However, at present, only linear mode APDs based on AlAsSb p-i-n structures have been reported [10]. An analysis of the Geiger performance of this material has yet to be investigated.

In this work, we investigate theoretically the performance advantages of AlAsSb based SPADs when compared to InP, InAlAs or Si.

II. MODEL DESCRIPTION AND VALIDATION

The device model is developed in commercial software, Silvaco Atlas [11]. Detailed modelled structure of AlAsSb p-i-n APD on InP substrate is shown in Table 1. The intrinsic region (w) ranging from 100 to 2000 nm is sandwiched between 300 nm p+ AlAsSb and 100 nm n+ AlAsSb cladding layers with top 20 nm and bottom 500 nm of InGaAs contact layers. The modelled structures are the same as reported in Ref. [9], [10], [12] and [13].

TABLE 1
SCHEMATIC STRUCTURE OF P-I-N DIODE

Material	Thickness (nm)	Doping (cm^{-3})	Purpose
In$_{0.53}$Ga$_{0.47}$As	20	1x10^{19}	p+ Contact
	300	2x10^{18}	p+ Cladding
Al$_{0.56}$As$_{0.44}$Sb	100 – 2000 nm	6x10^{15}	I (w)
	100	2x10^{18}	n+ Cladding
In$_{0.53}$Ga$_{0.47}$As	500	1x10^{19}	n+ Contact
InP Substrate (n+)			

Our model includes a set of fundamental physics equations which have been derived from Maxwell's laws and consist of Poisson's equation, the continuity equations and transport equation. Poisson's equation relates variations in the electrostatic potential to the local charge density. By solving the Poisson's equation and hence fitting the device capacitance-voltage (C-V) results, we can extract the background doping concentration and the peak electric field in the device. For example, Fig. 1 (a) shows our fitted C-V result for AlAsSb APD with w = 1000 nm and the obtained

background doping concentration for AlAsSb is 11x10^{15} cm^{-3}. We also apply the continuity and the transport equations to describe the electron and hole densities as a result of the drift-diffusion transport process, SRH generation–recombination and photo-absorption process. The absorption coefficients of InGaAs [14] and AlAsSb [10] are incorporated in the model to determine the light intensity absorption profiles. We further calculate the device avalanche multiplication at high reverse bias by incorporating the local impact ionization theory in the model. Impact ionization coefficients for AlAsSb are used as input parameters taken from Yi *et al*. [9]. Our simulated results show that the avalanche multiplication values for pure electron injection (λ = 420 nm) agree well with the experimental data for AlAsSb APDs with w between 100 and 1500 nm, as shown in Fig. 1 (b). Here, for the well-known dead-space effect, enabled impact ionization coefficients are used for AlAsSb APD with w = 100 nm and the electron and hole threshold energy are extracted with the values of 3.0 and 3.8 eV, respectively.

Since our model has demonstrated good agreement with AlAsSb APD performance in linear mode, we further investigate the Geiger mode operation in AlAsSb SPAD with ideal p-i-n structures. The device probability of breakdown (P_b) is calculated using line integrals of ionization rates along paths of the steepest potential gradient suggested by McIntyre [5]. Device breakdown voltage, V_{BD}, is determined at $P_b \approx$ 0.01. To validate our model, we carry out a comparison of the calculated P_b at different overbias ratios with the reported data [15] for InP SPAD with w = 1 and 2 μm under pure hole injection. From Fig. 2, it is clear to see that our modelled results are in good agreement with the reported values. The inset of Fig. 2 includes the calculated P_b at different reverse bias. Similar good agreement was also achieved for Si [16] and InAlAs [17] SPADs using our model. The carrier impact ionization rates of InP, InAlAs and Si are taken from Ref. [18], [19] and [20] respectively.

III. COMPARISON OF P_B IN DIFFERENT SPADs

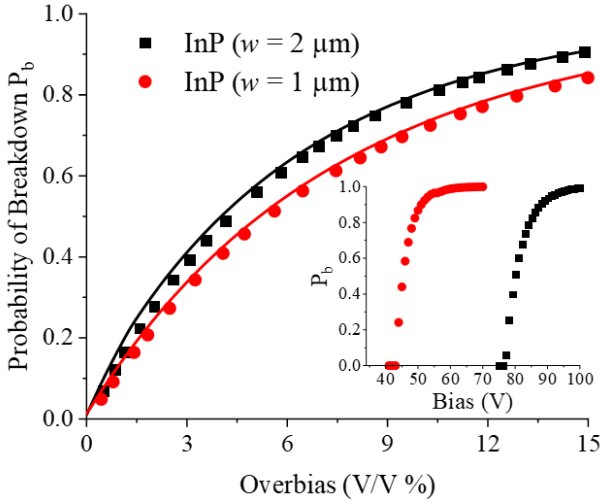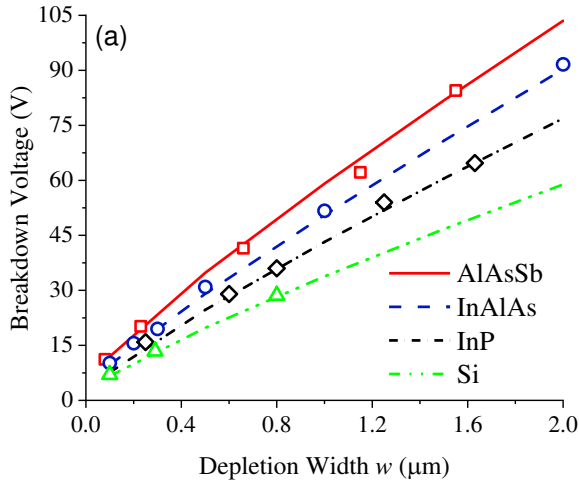Having validated our model, AlAsSb p-i-n SPADs with w

Fig. 2. Comparison of pure hole-initiated P_b for InP p-i-n diode with $w = 1$ μm and 2 μm calculated from our model (solid lines) and taken from Ref. [15] (symbols). Inset shows the corresponding calculated P_b vs. reverse bias.

ranging from 100 to 2000 nm are modelled considering pure electron injection. Fig. 3 (a) shows the calculated V_{BD} for AlAsSb SPADs with different w. The calculated V_{BD} values for InP (under pure hole injection), Si and InAlAs (under electron injection) with the similar p-i-n structures are also included for comparison. Our calculations show good agreement with the experimental data with a linear dependence of V_{BD} with w.

Fig 3 (b) shows the calculated P_b as a function of overbias ratio for AlAsSb SPADs. The P_b curves rise more abruptly for $w \geq 1000$ nm at overbias ratio $\leq 8\%$; however, the P_b increment is much slower with $w \leq 500$ nm, especially for that with $w = 100$ nm. For example, at 5% overbias ratio, AlAsSb SPAD with $w = 1500$ nm shows a P_b value of 0.81, which is significantly higher than that of 0.33 with $w = 100$ nm. Hence, AlAsSb SPADs with thicker w shows an advantage of higher P_b values. However, it is worth noting that a further increase of the overbias ratio above 8% does not yield substantial performance improvement for AlAsSb SPADs with $w \geq 1000$ nm as their P_b curves start to saturate.

The sharper P_b curves of thicker AlAsSb SPADs can be explained by analyzing the operating fields and corresponding α/β ratio for an overbias ratio of 5% as shown in Fig. 4. The operating field is ~1.07 MV/cm for a device with $w = 100$ nm while it is approximately half of the field value (~560 kV/cm) for $w = 2000$ nm. This leads to a significant increase of α/β ratio from ~3.9 to ~28.9, and thus results in a higher P_b value [5]. In addition, the lower operating fields in the thicker structure may have an additional advantage of lower tunneling currents and, thus, lower DCR. For devices beyond $w = 1500$ nm (corresponding to operating field ≤ 590 kV/cm), the α/β ratio does not increase significantly leading to only a minor improvement in P_b values (α/β ratio of ~22.3 and ~28.9 for $w = 1500$ and 2000 nm, respectively). Considering AlAsSb SPAD operation with high P_b (high SPDE) at low over bias ratio (low DCR) and the growth difficulty for thicker w because of the non-unity sticking coefficient of group V species (As, Sb) [24], [25], we deem the operating thickness for AlAsSb SPAD to be w between 1000 and 1500 nm.

Finally, we compare P_b values of AlAsSb SPAD with Si, InP and InAlAs SPAD at different overbias ratio. Fig. 5 (a) shows the calculated results for $w = 1500$ nm. Among the four types of SPADs, AlAsSb exhibits the sharpest rise in P_b curve. At an overbias of 5%, the calculated P_b value is 0.81, which is 0.18 and 0.28 higher than that for Si/InAlAs and InP respectively. To achieve $P_b = 0.81$ in InP, the overbias ratio of ~11% is necessary and the peak electric field increases from ~439 kV/cm to 463 kV/cm. This results in an order of magnitude increase of band-to-band tunneling current [26]. Donnelly et al. [27] reported that DCR of dummy InP SPADs (with $w = 1400$ nm and 1500 nm absorber) increases almost 10 times when the overbias voltage is increased from 4V to 10V corresponding to a P_b of ~0.51 and ~0.82 respectively. Since AlAsSb has a higher breakdown voltage than the rest of three materials, we also compare P_b for an alternative case at a fixed V_{BD}. Fig. 5 (b) shows an example of our calculated P_b at a fixed $V_{BD} \approx 60$ V (for AlAsSb SPAD with $w = 1000$ nm). AlAsSb still exhibits the highest P_b with a value of 0.74 at 5% overbias while it is 0.53 for InP.

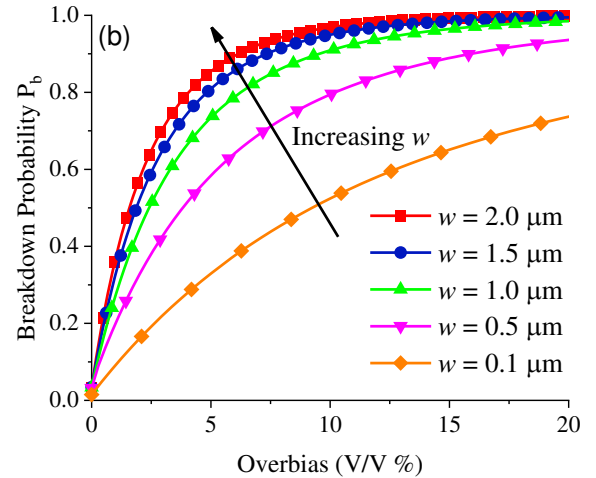The α/β ratios of the four devices at 5% overbias for w

Fig. 3. (a) Calculated (lines) and measured (symbols) breakdown voltage vs. depletion widths for AlAsSb [9], InP [21], [22], InAlAs,[19], [22] and Si [23]. (b) P_b vs. overbias for w ranging from 0.1 to 2 μm for AlAsSb.
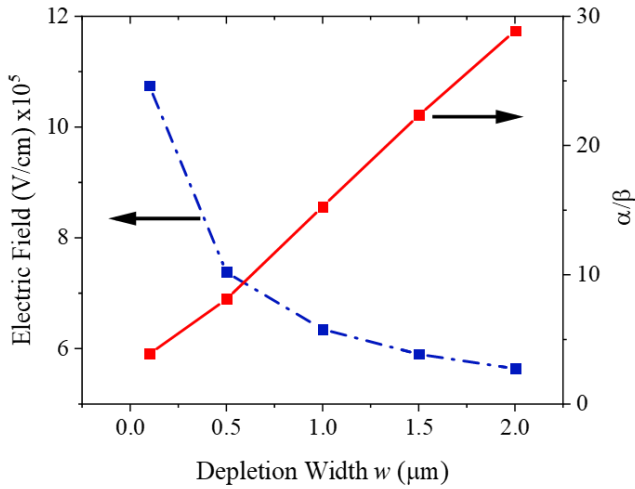
Fig. 4. Operating electric field and the corresponding α/β ratio vs. w at 5% overbias ratio.

=1500 nm and $V_{BD} \approx 60$ V are also shown in Fig. 5 (c). We can observe that AlAsSb has the largest α/β ratio among the four materials for both cases. There is an overall trend that a larger α/β ratio leads to a larger P_b value (hence higher SPDE), which is consistent with Ref. [5]. However, there is an exceptional case that, at w =1500 nm, Si and InAlAs show similar P_b values while Si has a larger α/β ratio (value of 4.6) than that of InAlAs (α/β ratio of 3). Comparison of ionization

coefficients of the four materials for their respective operating fields under consideration shows that InAlAs has more sharply increasing α and β than that of Si as shown in Fig. 5(d). This could explain a similar P_b value as Si at w =1500 nm [28].

In Fig. 5 (d), we can notice that AlAsSb operates at higher fields than the other three materials, but its higher indirect bandgap (~1.55 eV) results in a significantly lower band-to-band tunneling current [29] than both InAlAs and InP. For instance, no measurable band-to-band tunneling current was reported in AlAsSb APD at electric field up to 1.07 MV/cm [29], but the tunneling current density of ~10^{-3} and ~10^{-1} A/cm^2 were reported for InAlAs [19] and InP [26] respectively at field of 800 kV/cm. Hence, it is unlikely that the band-to-band tunneling mechanisms will dominate DCR in AlAsSb SPAD at the operating field up to ~800 kV/cm as shown in Fig. 5 (d). Fig. 6 shows an example of the measured dark current density (J_D) vs. the calculated peak electric field up to $0.9V_{BD}$ for AlAsSb devices with w = 1000 nm (up to 600 kV/cm) and w =1500 nm (up to 565 kV/cm) at 297 K and 77 K. The expected dark current (I_D) for a 25 µm diameter device is also indicated on the right y-axis, which is a typical size for III-V SPADs found in literature [30]. The measured J_D for both devices reduces by approximately 2-4 orders of magnitude when the operating temperature drops from 297 K to 77 K, suggesting that the devices are dominated by the surface leakage current instead of band-to-band tunneling
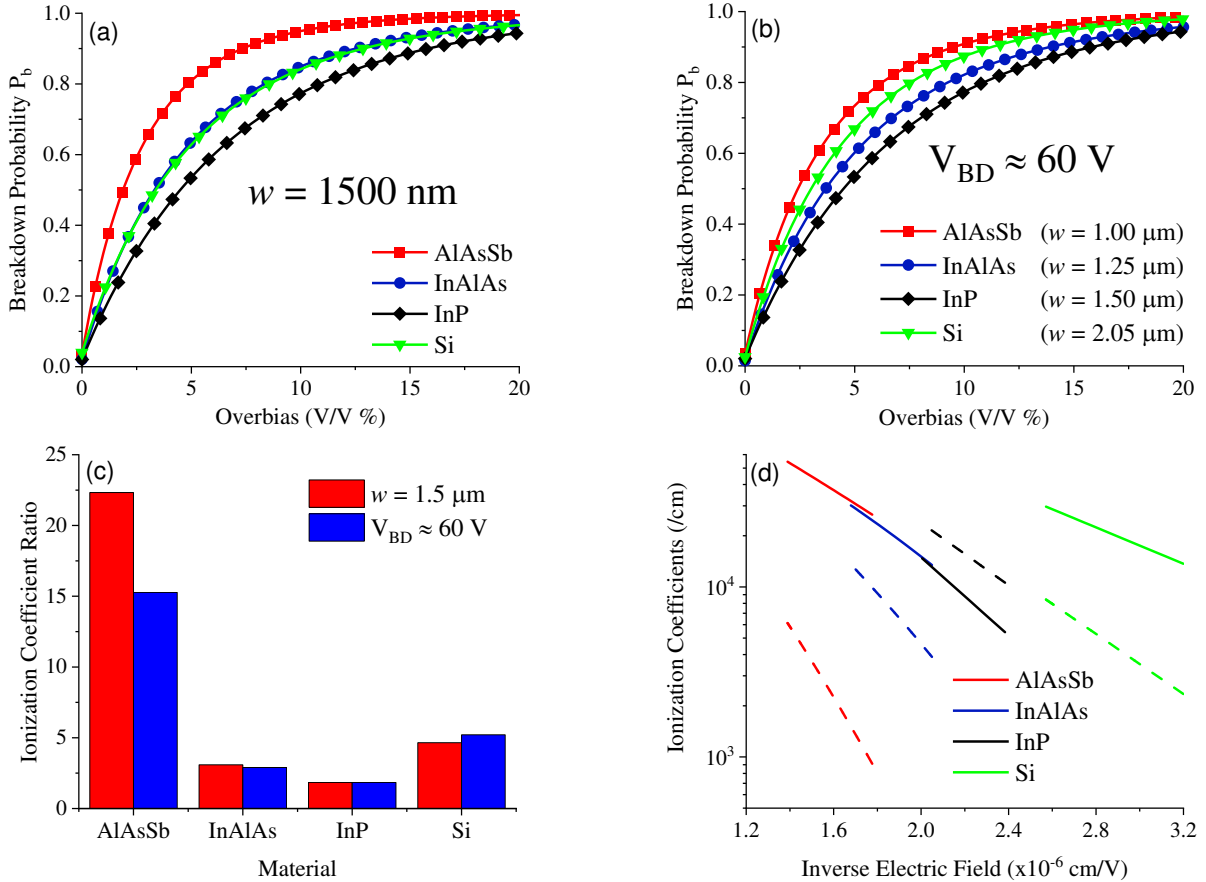

Fig. 5. (a) P_b vs. overbias ratio for w =1.5 µm, (b) P_b vs Overbias for fixed $V_{BD} \approx 60$ V, (c) α/β ratio at 5% overbias ratio the two cases of w = 1.5 µm and $V_{BD} \approx 60V$ for AlAsSb, InAlAs and InP and Si., (d) Ionization coefficients of electron(solid lines) and holes (dashed lines) vs inverse electric field
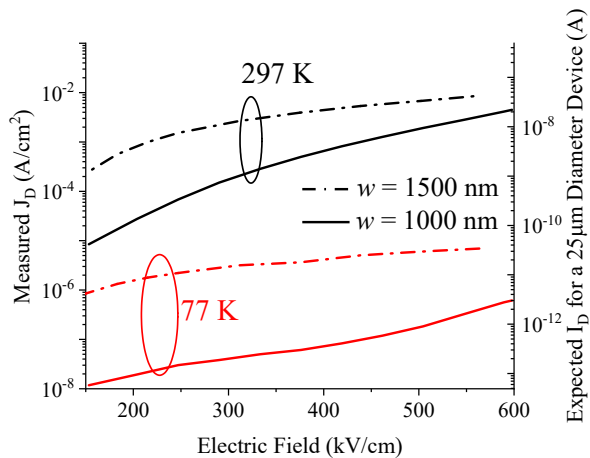
Fig. 6. Measured dark current density J_D vs. calculated electric field up to $0.9V_{BD}$ for AlAsSb devices with w = 1000 nm and 1500 nm at 297 K and 77 K. The right axis shows the expected dark current I_D for a 25 μm diameter device.

current. Our current devices with w =1500 nm show a high J_D of $7x10^{-6}$ A/cm^2 at 77 K; however, devices with w =1000 nm demonstrate $J_D \leq 6x10^{-7}$ A/cm^2 that corresponds to $I_D \approx 3$ pA at 77 K for a 25 μm diameter device at $0.9V_{BD}$. The higher dark current in our current AlAsSb devices with w =1500 nm may be due to the higher density of defects inside the multiplication layer and this variation was due to the different growth trials/time for different layer thickness. Nevertheless, further improvement of the as-grown material quality by reducing its defect density, and optimization of device processing such as improving etching and passivation recipe or utilizing planar structures to minimize the device leakage current, are necessary to achieve a low DCR SPAD with low afterpulsing. Together with the high P_b in AlAsSb, there is a potential for AlAsSb SPADs with high SPDE/DCR ratio at low overbias assuming similar generation mechanisms as observed in InP SPAD [6].

Temporal response is another important parameter to evaluate SPAD performance, however, it has not been included in this work yet as this functionality/module is not included in our Silvaco software. The timing jitter (the standard deviation of the mean time to breakdown) in SPAD deteriorates with larger α/β ratio but it improves with P_b [31]. Hence at similar low overbias ratio of ≤5%, we expect the timing jitter of AlAsSb SPAD can be comparable to InP SPAD for its much higher P_b.

IV. CONCLUSION

In this work, we presented a model for AlAsSb APD/SPADs. Comparison of experimental and modelling data for multiplication gain in AlAsSb APD shows excellent agreement at different multiplication region thicknesses. Model validation also includes the calculated P_b compared with the reported data for InP/InAlAs/Si SPADs. We demonstrate that AlAsSb SPAD, at both w of 1500 nm and a fixed V_{BD} value of 60V, shows higher P_b values compared

with Si, InAlAs and InP SPAD. This indicates a potential of higher SPDE/DCR ratio for AlAsSb SPAD at low overbias ratio of ≤5% if it is dominated by similar field-assisted tunneling current mechanisms as InAlAs and InP SPADs. However, further material quality control during epitaxy and device fabrication optimization and/or planar structures are still necessary for the operation of AlAsSb based SPAD. Our results suggest the high potential of utilizing AlAsSb as avalanche gain medium for SPAD applications.

REFERENCES

[1] N. Gisin, G. Ribordy, W. Tittel and H. Zbinden, "Quantum cryptography," Rev. Mod. Phys., vol. 74, no. 1, pp. 145–195, Mar. 2002.

[2] F. Stellari, A. Tosi, F. Zappa and S. Cova, "CMOS circuit testing via time-resolved luminescence measurements and simulations," IEEE Trans. Instrum. Meas., vol. 53, no. 1, pp. 163–169, Feb. 2004.

[3] A. McCarthy, X. Ren, A. Della Frera, N. Gemmell, N. Krichel, C. Scarcella, A. Ruggeri, A. Tosi, and G. Buller, "Kilometer-range depth imaging at 1550 nm wavelength using an InGaAs/InP single-photon avalanche diode detector," Opt. Express, vol. 21, no. 19, pp. 22098–22113, 2013.

[4] R. J. McIntyre, "Multiplication noise in uniform avalanche diodes," IEEE Tran. Electron Dev., vol. 13, no. 1, pp. 164-168, Jan. 1966.

[5] R. J. McIntyre, "On the avalanche initiation probability of avalanche diodes above the breakdown voltage," IEEE Tran. Electron Dev., vol. 20, no. 7, pp. 637-641, July 1973.

[6] M. A. Itzler, R. Ben-Michael, C. -F. Hsu, K. Slomkowski , A. Tosi , S. Cova , F. Zappa & R. Ispasoiu, "Single photon avalanche diodes (SPADs) for 1.5 μm photon counting applications," J. Mod. Opt., vol. 54, no. 2-3, pp. 283-304, Jan. 2007.

[7] J. C. Campbell, A. G. Dentai, W. S. Holden, and B. L. Kasper, "High-performance avalanche photodiode with separate absorption 'grading' and multiplication regions," Electron. Lett., vol. 19, no. 20, pp. 818–820, Sept. 1983.

[8] P. Vines, K. Kuzmenko, J. Kirdoda, D. C. S. Dumas, M. M. Mirza, R. W. Miller, D. J. Paul and G. S. Buller, "High performance planar germanium-on-silicon single-photon avalanche diode detectors," Nat. Commun., vol. 10, no. 1, pp. 1086, Mar. 2019.

[9] X. Yi, S. Xie, B. Liang, L. W. Lim, X. Zhou, M. C. Debnath, D. L. Huffaker, C. H. Tan and J. P. R. David. "Demonstration of large ionization coefficient ratio in AlAs$_{0.56}$Sb$_{0.44}$ lattice matched to InP," Sci. Rep., vol. 8, no. 1, pp. 9107, Jun. 2018.

[10] X. Yi, S. Xie, B. Liang, L. W. Lim, J. S. Cheong, M. C. Debnath, D. L. Huffaker, C. H. Tan and J. P. R. David. "Extremely low excess noise and high sensitivity AlAs0.56Sb0.44 avalanche photodiodes". Nat. Photonics, vol. 13, no. 10, pp. 683–686, July 2019.

[11] https://www.silvaco.com/products/tcad/device_simulation/atlas/atlas.html (2019).

[12] C. H. Tan, S. Xie and J. Xie, "Low noise avalanche photodiodes incorporating a 40 nm AlAsSb avalanche region," IEEE J. Quantum Electron., vol. 48, no. 1, pp. 36-41, Jan. 2012.

[13] J. Xie, S. Xie, R. C. Tozer and C. H. Tan, "Excess noise characteristics of thin AlAsSb APDs," in IEEE Tran. Electron Dev., vol. 59, no. 5, pp. 1475-1479, May 2012.

[14] S. M. Kelso, D. E. Aspnes, M. A. Pollack, and R. E. Nahory, "Optical properties of In$_{1-x}$Ga$_x$As$_y$P$_{1-y}$ from 1.5 to 6.0 eV determined by spectroscopic ellipsometry," Phys. Rev. B., vol. 26, no. 12, pp. 6669-6681, Dec. 1982.

[15] J. S. Ng, C. H. Tan, G. J. Rees and J. P. R. David, "Effects of dead space on breakdown probability in Geiger mode avalanche photodiode," J Mod. Opt., vol. 54, no. 2-3, pp. 353-360, Jan. 2007.

[16] J. D. Petticrew, S. J. Dimler, X. Zhou, A. P. Morrison, C. H. Tan and J. S. Ng, "Avalanche breakdown timing statistics for silicon single photon avalanche diodes," IEEE J. of Sel. Top. Quantum Electron., vol. 24, no. 2, pp. 1-6, Mar. 2018.

[17] S. Wang, F. Ma, X. Li, G. Karve, X. Zheng, and J. C. Campbell, "Analysis of breakdown probabilities in avalanche photodiodes using a history-dependent analytical model," Appl. Phys. Lett., vol. 82, no. 12, pp. 1971-1973, Mar. 2003.

[18] L. W. Cook, G. E. Bulman, and G. E. Stillman, "Electron and hole impact ionization coefficients in InP determined by photomultiplication measurements," *App. Phys. Lett.*, vol. 40, no. 7, pp. 589–591, Apr. 1982.

[19] Y. L. Goh, D. J. Massey, A. R. J. Marshall, J. S. Ng, C. H. Tan, W. K. Ng, G. J. Rees, M. Hopkinson, J. P. R. David and S. K. Jones, "Avalanche multiplication in InAlAs," *IEEE Trans. Electron. Dev.*, vol. 54, no. 1, pp. 11–16, Jan. 2007.

[20] R. V. Overstraeten, and H. D. Man, "Measurement of the ionization rates in diffused silicon p-n junctions," *Solid-State Electron.*, vol. 13, no. 5, pp. 583–608, May 1970.

[21] L. J. J. Tan, J. S. Ng, C. H. Tan, M. Hopkinson and J. P. R. David, "Effect of dead space on Low-Field avalanche multiplication in InP," *IEEE Tran. Electron. Dev.*, vol. 54, no. 8, pp. 2051-2054, Aug. 2007.

[22] L. J. J. Tan, D. S. G. Ong, J. S. Ng, C. H. Tan, S. K. Jones, Y. Qian and J. P. R. David, "Temperature dependence of avalanche breakdown in InP and InAlAs," *IEEE J. Quantum Electron.*, vol. 46, no. 8, pp. 1153-1157, Aug. 2010.

[23] D. J. Massey, J. P. R. David and G. J. Rees, "Temperature dependence of impact ionization in submicrometer silicon devices," *IEEE Trans. Electron. Dev.*, vol. 53, no. 9, pp. 2328-2334, Sept. 2006.

[24] E. Hall, H. Kroemer, and L. A. Coldren, "Improved composition control of digitally grown AlAsSb lattice-matched to InP," *J. Cryst. Growth*, vol. 203, no. 3, pp. 447–449, Jun. 1999.

[25] Y. H. Zhang, "Accurate control of As and Sb incorporation ratio during solid-source molecular-beam epitaxy," *J. Cryst. Growth*, vol. 150, no. 2, pp. 838–843. May 1995.

[26] L. J. J. Tan, J. S. Ng, C. H. Tan and J. P. R. David, "Avalanche Noise Characteristics in Submicron InP Diodes," in *IEEE Journal of Quantum Electronics*, vol. 44, no. 4, pp. 378-382, April 2008

[27] J. P. Donnelly, E. K. Duerr, K. A. Mcintosh, E. A. Dauler, D. C. Oakley, S. H. Groves, C. J. Vineis, L. J. Mahoney, K. M. Molvar, P. I. Hopman, K. E. Jensen, G. M. Smith, S. Verghese and D. C. Shaver, "Design Considerations for 1.06-μm InGaAsP–InP Geiger-Mode Avalanche Photodiodes," *IEEE J. Quantum Electron.*, vol. 42, no. 8, pp. 797-809, Aug. 2006

[28] J. S. Ng, C. H. Tan and J. P. R. David, "A comparison of avalanche breakdown probabilities in semiconductor materials", *J. Mod. Opt.*, vol. 51, no 9-10, pp. 1315-1321, Jun. 2004.

[29] S. Xie and C. H. Tan, "AlAsSb avalanche photodiodes with a Sub-mV/K temperature coefficient of breakdown voltage," *IEEE J. Quantum Electron.*, vol. 47, no. 11, pp. 1391-1395, Nov. 2011.

[30] M. A. Itzler, X. Jiang, M. Entwistle, K. Slomkowski, A. Tosi, F. Acerbi, F. Zappa & S. Cova, "Advances in InGaAsP-based avalanche diode single photon detectors," *J. Mod. Opt.*, vol. 58, no. 3-4, pp. 174-200, Jan. 2011.

[31] C. H. Tan, J. S. Ng, G. J. Rees and J. P. R. David, "Statistics of Avalanche Current Buildup Time in Single-Photon Avalanche Diodes," *IEEE J. of Sel. Top. Quantum Electron.*, vol. 13, no. 4, pp. 906-910, July-Aug. 2007.

Fellowship Program (until to Mar. 2021), leading and developing a novel antimony-based solid-state material system and sensors.

Dr. Baolai Liang received his Ph.D. degree in Microelectronics-Photonics from the University of Arkansas. He is now the director of Integrated Nanomaterials Laboratory at the California NanoSystems Institute, the University of California - Los Angeles. His main research interests include molecular beam epitaxy growth and optical characterizations of low-dimensional III-V semiconductor materials for optoelectronics device applications

Dr. Xin Yi obtained the B.Eng and Ph.D. degrees in Electronic and Electrical Engineering from the University of Sheffield, Sheffield, U.K., in 2015 and 2020, respectively. He is currently a research associate with Heriot-Watt University, Edinburgh, U.K. His research interests include ultrahigh-speed avalanche photodiode, single-photon avalanche diodes and LiDAR.

Mr. Xiao Jin obtained the BEng degree in Electronic Electrical Engineering from University of Sheffield in 2018. He is currently a PhD candidate in semiconductor group in University of Sheffield. His research is focused in characterization of III-V semiconductor material and devices, especially that AlAsSb/AlGaAsSb material system. He is studying the impact ionization process via different modelling techniques and look experimentally at the ionization coefficient in different semiconductor materials and device structures. The aim of my PhD research is to develop ADPs capable of operating at very high speeds and high sensitivity for next generation telecommunication networks.

Dr. Manoj Kesaria received the PhD degree from Jawaharlal Nehru Centre for Advanced Scientific Research, Bangalore, India, in 2012. Between 2012-18, he has worked at the Universities of Houston, Lancaster, and Sheffield. He is currently a Lecturer/Assistant Professor at the School of Physics and Astronomy at Cardiff University (CU). He is presently involved in novel compound semiconductor development, epitaxy, fabrication, and characterisation of detectors, LED and Thermophotovoltaics (TPV).

Prof. John P.R. David obtained his B.Eng. in Electronic Engineering and Ph.D. from the University of Sheffield in 1979 and 1983 respectively. Between 1982–2001 he was a postdoctoral researcher working in the same Department on the study of impact ionisation coefficients and III-V materials characterisation. Between 2001-2002 he was a senior engineer with Bookham Technologies before returning to Sheffield University as a Senior Lecturer. During 2002-2004 he was an IEEE LEOS Distinguished Lecturer, giving presentations on the topic of 'Low Noise Avalanche Photodiodes'. He has published in excess of 350 journal papers, and has a similar number of conference presentations in the areas of avalanche photodiodes, impact ionisation and III-V material characterisation. He is a Fellow of the IET and IEEE.
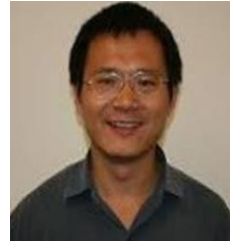
Mr. Jamal Ahmed received the B.Eng. degree from the Department of Electrical Engineering, National University of Sciences and Technology, Pakistan, in 2013 and the MSc degree in Smart Systems Integration from School of Engineering and Physical Sciences, Heriot-Watt University, UK in 2018. He is currently pursuing the Ph.D. degree with the University of Cardiff, Cardiff, U.K focusing on impact ionization properties of III-V materials and avalanche photodiodes for optical communication applications.

Dr. Shiyu Xie received the B.S. degree from Huazhong University of Science and Technology, Wuhan, China, in 2007, and the Ph.D degree in Electronic and Electrical Engineering, University of Sheffield, UK, in 2012. From 2012 to 2014, she was with Huawei Corporation as a Research Engineer. From 2014 to 2016, she was postdoctoral fellow at Sheffield and Cardiff University respectively. Since 2017, she is a research fellow at Cardiff sponsored by the European Regional Development Fund through Welsh government Ser Cymru

Prof. Diana L. Huffaker (FIEEE, FOSA, FLSW) was the Welsh Government Sêr Cymru Chair in Advanced Materials and Engineering. She was Science Director for the Institute for Compound Semiconductors (ICS) with considerable experience in managing large, multi-institutional programmers supported by the US National Science Foundation, Department of Defence etc. Since Aug. 2020, She is chair of the Electrical Engineering Department at UT Arlington. She is a pioneer in MBE growth of III-Sb bulk and quantum dot materials and recently demonstrated growth of sb material using the DA technique. Her research expertise includes novel III-As,Sb epitaxial methods, fabrication and high performance detectors.